Experiments in Fluids 8, 1–12 (1989)

Experiments in Fluids

The turbulent flow field around a circular cylinder

B. Dargahi

Hydraulics Laboratory, The Royal Institute of Technology, S-100 44 Stockholm, Sweden

Abstract. The flow field around a circular cylinder mounted vertically on a flat bottom has been investigated experimentally. This type of flow occurs in several technical applications, e. g. local scouring around bridge piers. Hydrogen bubble flow visualization was carried out for Reynolds numbers ranging from 6,600 to 65,000. The main flow characteristic upstream of the cylinder is a system of horse-shoe vortices which are shed quasi-periodically. The number of vortices depends on Reynolds number. The vortex system was found to be independent of the vortices that are shed in the wake of the cylinder. The topology of the separated flow contains several separation and attachment lines which are Reynolds number dependent. In the wake region different flow patterns exist for each constant Reynolds number.

List of symbols

B	width of flume
b_0	wake width
C_d	drag coefficient
C_f	coefficient of skin friction
C_p	pressure coefficient
D	cylinder diameter
Ks	bed roughness
L_E	integral length scale
Re	Reynolds number based on Ym
$Re\,(D)$	Reynolds number based on D
$Re(l)$	Reynolds number based on length
U	free stream velocity
Um	mean flow velocity
$U_{s,\max}$	maximum velocity deficiency
u	streamwise velocity
u_*	shear velocity
X, Y, Z	cartesian co-ordinate system measured from the cylinder centre
X, Y, Z	longitudinal, vertical and lateral directions
Ym	mean flow depth
δ	boundary layer thickness
Γ	circulation
δ_d	displacement thickness
θ	momentum thickness
λ_f	dissipation length scale
ν	kinematic viscosity
Ω	vorticity
τ	shear stress

1 Introduction

The flow field in a shear flow around a circular cylinder mounted vertically on a flat wall is essentially a three-dimensional separated boundary layer flow. This type of flow has many different aspects which interact in a complicated manner. The complication is a result of interaction between the two-dimensional approaching boundary layer flow and the adverse pressure gradient set up by the cylinder. Cases of such three-dimensional problems occur rather frequently in engineering practice, e. g. in the flow field in turbo-machinery, axial compressors and local scouring around bridge piers. A vast amount of experimental works exists on the problem of local scouring. However, in most of these studies the emphasis has been on the formulation of scour-depth equations rather than on the mechanism of local scouring (Dargahi 1983). The mechanism has to be investigated in terms of the flow field and its interaction with the mobile bed before and during scouring.

The main flow characteristics around a cylinder are a relatively large secondary flow region and skewed velocity distributions. The skewing is caused by the pressure gradient normal to the main flow direction. The boundary layer upstream of the cylinder must overcome a strong pressure gradient set up by the cylinder. This leads to separation of the flow. In the separated region a vortex system is developed which is stretched around the cylinder like a horse-shoe. There are fundamental differences between the three-dimensional boundary layer separation and the counterpart in two-dimensional flows. In the latter case the universally accepted features of separation are: a streamline leaves the surface at a point where there is a reversed flow and the wall shear stress is zero. In the former case the limiting streamline at the wall does not leave the surface and the wall shear stress is finite everywhere, except at so-called singular points. There are two general concepts which form the basis of the understanding of the physics of three-dimensional separated flows: the concept of limiting streamlines and the critical

point theory. The former concept has been developed by Maskell (1955) and the latter by Lighthill (1963). The critical point theory has been further modified and applied to many different flow problems by: Perry and Fairlire (1974), Hunt et al. (1978), Tobak and Peake (1982), Dallmann (1983), Perry and Steiner (1987). Despite the differences in definition of separation and the terminology used, it seems possible to summarize the main characteristics of three-dimensional boundary layer separation as follows:

(1) Convergence of limiting streamlines (or skin-friction lines) to a particular line is a necessary condition for separation. Such a line can conveniently be called an open-bifurcation line.
(2) Three-dimensional separated flows are normally composed of a complex system of vortices in which no bubble type separation can survive.
(3) The critical point theory provides a means by which many complicated flow patterns can be analysed, using only the geometric understanding of the critical points and their relation with the flow field as a whole.
(4) Two flow fields are topologically identical if they show the same distribution of critical points.
(5) A structurally unstable pattern behaves as a source from which a number of different stable and unstable patterns develop.

The complexity of the flow field around a circular cylinder makes theoretical, experimental, as well as numerical methods rather complicated for this case. Flow visualization techniques provide a means by which the problem can be investigated qualitatively. Schwind (1962) investigated the three-dimensional boundary layer separation upstream of a triangular strut placed in a wind tunnel. The visualizations were carried for low Reynolds numbers (laminar). The results found were compatible with Maskell's general description. He found that the primary upstream separation distance increases with Re. In the separated region, five different flow regimes were recognized in order of increasing Reynolds number. Regime 1 (lowest Re) no vortices were found. Regimes 2, 3 and 4 were characterized by 1 open vortex, 2 open vortices and 2 vortices, respectively. The vortices were shed periodically. In regime 5 the vortex system moved forward and backward close to the bed. Roper (1967) used hydrogen bubble method to study the flow field around a circular cylinder for $Re(D)$ ranging from 2,740 to 3,180. He also observed that the horse-shoe vortices have a periodical character. Belik (1973) investigated the flow field upstream of a cylinder for $Re(D)$ ranging from 36,000 to 220,000. He proposed an empirical expression to estimate the position of the separation line. He also concluded that for both laminar and turbulent flows the separation region is characterized by the Reynolds number based on the boundary layer thickness. Goldstein (1984) carried out detailed measurements of mass transfer from a cylinder. The results of his measurements at $Re(D) = 19{,}000$ indicated a close relation between the horse-shoe vortex system and mass transfer characteristics. A small vortex located near the cylinder was found to cause high values of Sherwood number.

The character of the horse-shoe vortex system depends on the diameter of the cylinder, the mean flow depth, the velocity, the bed roughness and the boundary layer thickness. We have the following dimensionless parameters

Ym/δ, D/δ, Ks/δ, and $Re(D)$.

In this paper a study of the turbulent flow field for the case of fixed bed, which simulates the condition before scouring, is presented. The objectives were to investigate by means of flow visualization and flow measurements, the dynamics of the vortex system around the cylinder, the mutual interaction of the horse-shoe and wake vortices, the problem of separation and the main flow characteristics. The flow field in the wake of a circular cylinder mounted normal to a flat wall is modified by the additional effect of the wall boundary layer. It is believed that the vortex shedding, the location of the separation line at either side of the cylinder and the basic flow parameters are somewhat different from those observed for the case of a two-dimensional flow.

2 Experiments

2.1 Experimental set up and measuring technique

All the experiments were conducted in a 22 m long, 1.5 m wide and 0.65 m deep recirculating hydraulic flume. The mean velocity distributions were measured along the centre line of the flume at various stations. At non-dimensional distances $X/Ym > 80$ (measured from the inlet), the distributions were well described by the logarithmic law of the wall. The spanwise velocity distributions also showed a reasonable uniformity. A circular cylinder of 0.15 m diameter and 0.5 m height was mounted vertically on the flume bed along the centre line at a distance of 18 m from the inlet. The cylinder was rigidly fixed to the bed. A uniformly graded fine sand of mean diameter $D_{50} = 0.36$ mm was glued to the bed giving a slight surface roughness. The roughness height in wall units was approximately 4.5, implying that the surface was practically smooth. The turbulent boundary layer extended across the entire flow depth for all the experiments. The flow was visualized by means of hydrogen bubble technique using a gold wire of diameter 0.05 mm, for Reynolds numbers ranging from 6,600 to 65,000 ($Re(D) = 8{,}400$ and 46,000). Detailed measurements of the key variables of the flow, such as pressure, velocity distribution and bed shear stresses were made at $Re(D) = 39{,}000$. Hot film anemometry was used to study the turbulent characteristics of the flow, and a HP 9836 computer was utilized for data acquisition and analysis.

Pressure measurements were carried out using a differential pressure transducer which could register fluctuations up to 25 Hz with good accuracy. The pressure transducer was calibrated before each measurement. Hot-film DISA type anemometer (55D01) was utilized for both velocity and turbulence measurements. Only one component measurements were made. Before and after each experiment, the probes

were calibrated in a submerged jet of a calibration apparatus designed specially for this purpose. The same water was supplied both to the calibration apparatus and the flume. The bed shear stresses were measured indirectly by means of a pitot tube, using Preston method (Preston 1954) with the universal constants given by Patel (1965).

Various statistical moments, auto-correlation, frequency spectrum and turbulent scales were computed from the instantaneous velocity signals. For these computations, test of periodicity and stationarity were carried out on the raw data. For turbulence analysis, low frequency fluctuations were removed by means of suitable recursive digital filters.

In the separated flow region where a flow reversal takes place, most of the standard methods cannot be used. In the present study, hot film anemometry in combination with flow visualization was used. Visualization revealed the local flow direction. Where possible, the measuring probes were aligned in both main and reversed flow directions. The velocity signals were then analysed in order to find the portion of time for which the flow was reversed. The measurements were repeated with different types of hot-films. The results obtained were remarkably consistent.

2.2 Accuracy and reliability

The uncertainty associated with velocity measurements by means of hydrogen bubble visualization was evaluated by the method described by Schraub et al. (1965). The uncertainty in measuring the locations of bubble was found to be about 4%. The total error in velocity measurements was estimated as 7.5%.

The total maximum error in differential pressure measurements was 3%. This includes the errors introduced by misalignment, wall effects, turbulence, geometry of the probes and calibration uncertainties. The maximum error for hot-film measurements was estimated as 4.5%. The error associated with bed shear stress measurements was found from the method given by Patel (1965) which amounted to about 3–6%. All the measurements could be repeated with good accuracy.

The accuracy and reliability of the measurements carried out in the reversed flow regions are lower than in the other regions of the flow and they must be taken with some reservation.

3 Results and discussion

3.1 Flow visualization: upstream region

For Reynolds numbers $Re\,(D)$ ranging from 20,000 to 39,000 the vortex system in the upstream separated region consists of at least five vortices which are shed quasi-periodically and have a shape similar to a horse-shoe in a plan view. Figure 1 a and b shows the vortex system in a vertical plane

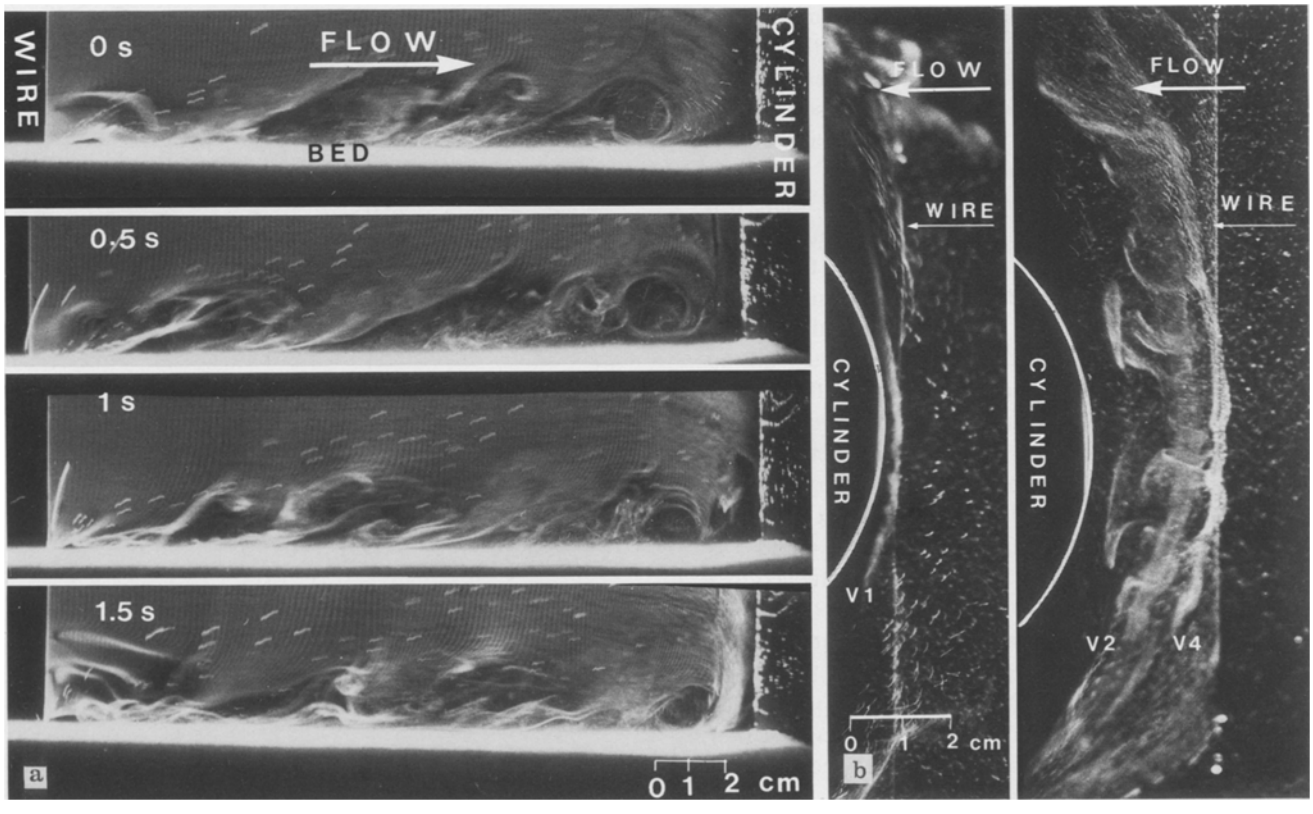

Fig. 1. a The horse-shoe vortex system in the plane of symmetry upstream of the cylinder at $Re(D) = 20{,}000$; wire position: $X/D = -1.83$ and $Z/D = 0$; **b** the horse-shoe vortex system in a horizontal plane close to the bed ($y/Ym = 0.005$), upstream of the cylinder at $Re(D) = 20{,}000$

along the line of symmetry and in a horizontal plane close to the bed at $Re = 20{,}000$. The vortex formation can be readily described by means of a general pattern as shown in Fig. 2. The downward flow at the stagnation face of the cylinder separates from the surface and a very small vortex in anti-clockwise direction (against the main flow direction) is created, here denoted as vortex 1. The flow from the lower part of the boundary layer is turned up into a clockwise vortex (vortex 2). A small triangular anti-clockwise vortex is formed as the next layer of fluid separates from the lower part of vortex 2. Its formation is in accordance with the fact that the neighbouring vortices always rotate in opposite directions. A fraction of second after the formation of vortex 2 (when the flow is started from rest), an instability occurs at its upstream end which grows in size and finally develops into a fourth vortex rotating in clockwise direction. Subsequent to the formation of vortex 4, a fifth vortex develops upstream and close to vortex 4. Vortex 5 seems to be a product of the interaction of the initial instability and a jet of fluid caused by acceleration of a thin boundary layer underneath vortex 2. Vortex 5 rotates in anti-clockwise direction. The quasi-periodic sequence of the vortex formation starts with the detachment of vortex 2. Vortex 2 then becomes a closed vortex and as it is convected downstream its cross-sectional area decreases as it is stretched (Fig. 1 a). Next it moves quickly along the bed, away from the cylinder. It then either moves into vortex 4 or it is dissipated upstream of vortex 3 in the secondary flow region. As the horse-shoe vortices interact with each other in a complicated manner. A complete description of their movement is not possible. Nevertheless, the simple idea of vortex image can be used to describe the dynamics of the vortices in general terms. The description is based upon a potential vortex assumption. A similar approach was adapted by Schwind (1962).

As vortex 2 is convected towards the cylinder, there will be also an influence of its image in the cylinder, pushing the vortex down towards the bed. As it approaches the bed, it moves back upstream under the influence of its image in the bed. Since the rate of change of circulation balances the diffusion of vorticity, the circulation of the vortex has to decrease, as during its movement, its vorticity is diffused. The movement of vortex 2 also influences the other vortices. As vortex 3 is formed from vortex 2, it too is convected downstream. This causes the vortex pair 4 and 5 to rise up due to weakened influence by the neighbouring vortex 3. When vortex 3 moves back upstream, the vortex pair 4 and 5 is pressed down towards the bed. They are then detached in a manner similar to vortex 2.

The horse-shoe vortices are shed with different periodicities. At $Re(D) = 39{,}000$ the shedding frequencies vary from 0.1 to 2 Hz. This may be compared with the frequency 0.32 Hz given by Strouhal number. This could suggest that the two phenomena of the upstream vortex shedding and wake vortex shedding are related. In order to investigate this problem, the wake was eliminated by means of an elongated cylinder (2 m long). The flow visualization results were almost identical to those found for the case of the circular cylinder. Hence, its seems that the influence of wake vortices on the upstream vortex system is rather weak.

At $Re(D) = 39{,}000$, the position of the upstream separation point oscillates about a mean location of $X/D = -0.83$, along the line of symmetry. This value is comparable to the values of -0.72 and -0.85 found by Belik (1973) and Melville (1975), respectively at Reynolds numbers of the same range as in the present study. The separation surface intersects the bed along a circular arc within the range $-70°$ to $70°$. The bed shear stresses only vanish at the singular points which are located along the line of symmetry upstream of the cylinder. As Re increases from 6,600 to 65,000, the primary separation distance increases from $X/D = -0.73$ to $X/D = -0.93$. This conclusion agrees with Schwind's (1962) results. The size and position of vortex 2 seems to be independent of Re. The macro scale in the secondary flow region must then depend essentially on the diameter of the cylinder. The number of vortices also increases from 2 to 9 as Re increases from 6,600 to 65,000, respectively.

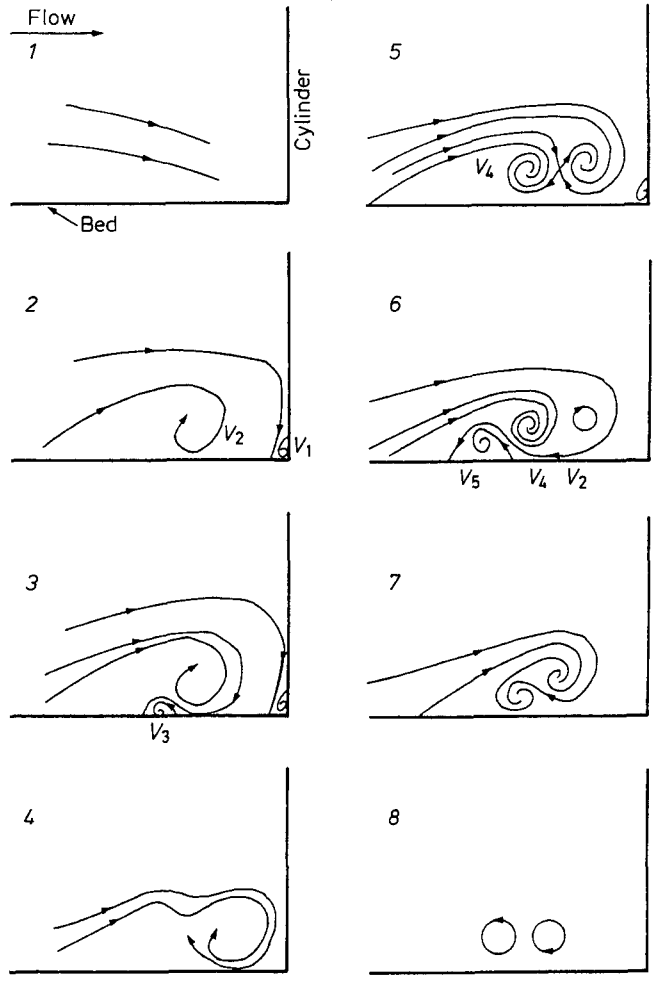

Fig. 2. The sequence of vortex formation in the plane of symmetry upstream of the cylinder at $Re(D) = 20{,}000$

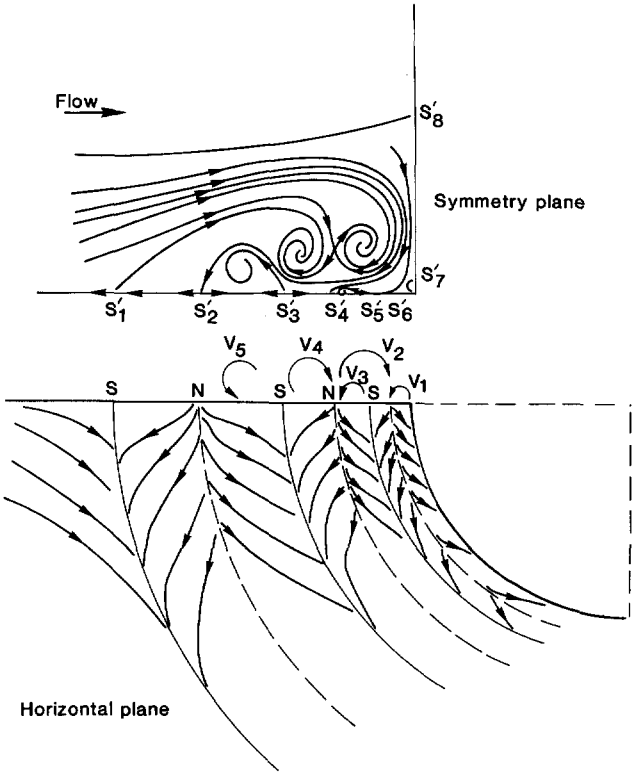

Fig. 3. The topological structure of the flow upstream of the cylinder at $Re(D) = 20{,}000$

3.2 *Topological structure of the flow*

The mean streamline patterns along the plane of symmetry upstream of the cylinder is shown in Fig. 3a. The patterns are derived from the flow visualization results at $Re(D) = 20{,}000$. The topological structure of the flow consists of eight half-saddle points (S') at the bed and at the vertical face of the cylinder, five vortices which are considered as nodal points (N) and an inviscid saddle critical point (S) which occurs above the bed between vortices 2 and 4. The number of half-nodal point (N') is equal to zero. These critical points satisfy the topological law given by Hunt et al. (1978), i.e.

$$(\Sigma N + \Sigma N'/2) - (\Sigma S + \Sigma S'/2) = 0 \qquad (1.1)$$

so that

$$(5 + 0) - (1 + 8/2) = 0.$$

The skin-friction patterns in a horizontal plane close to the bed, were deduced from the mean streamline patterns at the plane of symmetry. The patterns are illustrated in Fig. 3b. The topology of the skin-friction consists of a combination of saddle-nodal-saddle critical points. The main features of the flow structure in both the planes can be summarized as follows:

(1) There is no closed region of separated flow known as bubble type separation.

(2) No streamline can be recognized as a "surface envelope" line.

(3) There are three separation and three attachment lines. These can be identidied as negative and positive bifurcation lines, respectively (Perry and Steiner 1987, Fig. 1j and k).

(4) The "separated" flow over the upper part of the secondary flow region does not reattach. The streamlines that leave the bed wind themselves into vortices (or focus) which are stretched around the cylinder into horseshoe type vortices. All the five vortices are of stable focus type (Perry and Steiner 1987, Fig. 1g). Vortices 1, 3 and 5 can be classified as the "elementary structure" occurring at $0 < \lambda < 4/5$ (Dallmann 1983, Fig. 7), λ was defined as a stability parameter and is a function of the wall shear stress components. Dallmann found unstable structural configurations to occur at values $\lambda = 0$ and 1.

The topological structure just described, corresponds to the condition when all the vortices exist at the same time. However, as the vortices have a periodical character, different topological structures are created at each stage of the shedding cycle of the vortices. Hence, from the stability point of view, the horse-shoe vortex system is not a stable structure.

3.3 *Flow visualization: downstream region*

The main flow feature in the wake of the cylinder for the case of a two-dimensional flow, is the existence of the well known vortices (primary) which are shed at Strouhal frequency. However, as the flow is affected by the rigid boundary of the bed, the motion is fully three-dimensional and differences arise between the 2-D and 3-D cases. Some of the main differences are discussed. In the range of Reynolds number investigated, the primary vortices are shed periodically with a constant frequency, within the relative flow depth $y/Ym = 0.1-0.9$. The frequency values are almost identical to those predicted by standard Strouhal numbers. Close to the bed the vortices are shed at different frequencies. Near the bed in the region $X/D < 8$, the turbulent character of the wake is amplified and the width of the wake decreases. The latter effect can also be due to the acceleration of flow near the bed, towards the centre of the wake where the pressure is low. The primary vortices are convected downstream by the mean shear flow and they are eventually diffused. The outside edges of the vortices are ahead of the inside one due to the mean velocity gradient which deforms the vortices into an elliptical shape.

In addition to the primary wake vortices a different type of vortices known as secondary vortices were observed. These vortices originate from the separated region of the boundary layer at the two sides of the cylinder and they are symmetrically shed. They appear as instabilities superimposed on the large scale separation at the sides of the cylinder and they are similar to boundary layer stability waves. The frequency ratio of the secondary vortices to the primary

vortices was estimated to be about 100 for $Re(D) = 39{,}000$. The same type of vortices were observed by Wei and Smith (1986). The amplification of these vortices by three-dimensional effect can be the cause of transition to turbulent flow.

The position of the separation line at the sides of the cylinder is also affected by the solid bed boundary. Within the relative flow depth (y/Ym) range of 0.1–0.9, the separation line is located at 80° (measured from forward stagnation point) as predicted for a 2-D case. However, near the bed, the separation line moves further downstream reaching a value of 90° at the bed. The effect is analogous to that achieved by mounting a thin ring around a sphere, and is caused by the increased turbulence level near the bed.

The flow field immediately downstream of the cylinder in a vertical plane was also investigated, the results showed that in the range of $Re(D) = 8{,}400$–$46{,}000$ different flow patterns exist for each constant Reynolds number. As an example three different flow patterns exist at $Re(D) = 39{,}000$. The flow direction varies with time, the change from one pattern to the other takes place periodically at Strouhal frequencies. Different flow patterns are created as packets of low or high pressures migrate from one region of the flow to the other.

3.4 Flow measurements: upstream region

The flow measurements were carried out at a constant Reynolds number, $Re(D) = 39{,}000$. The basic flow conditions are given in Table 1.

3.4.1 Pressure

Figure 4 shows the pressure distribution upstream of the cylinder along the line of symmetry. The deviation of the experimental values from potential theory starts at about $X/D = -0.85$. This value is close to the mean position of the primary separation point found by flow visualization. In the range $-0.8 < X/D < -0.68$, the distribution exhibits a more or less constant value. The existence of this plateau is attributed to the smoothing effect of the horse-shoe vortices i.e. vortices 2–5. Vortex 1 seems to have no influence on the pressure distribution. The experimental data agree well with results found by Belik (1973) at $Re(D) = 10^6$ and $D = 30$ mm. The pressure distribution was found to be relatively insensitive to the change in Reynolds number. This conclusion is further supported by Belik's results, as he obtained the same type of distribution in the super-critical range. At very low Reynolds numbers the pressure coefficient, Cp is expected to decrease as $Re(D)$ and D/δ decrease. The pressure distribution downstream of the cylinder along the centre line of the flume showed a significant increase in the region close to the cylinder. The increase is probably caused by the primary wake vortices. The pressure distributions were also measured along the vertical face of the cylinder at intervals of 30°. Figure 5 shows the mean distribution along the upstream stagnation line. The figure illustrates the existence of a pressure gradient which is caused by the non-uniform velocity distribution of the approach flow. The pressure gradient causes a local boundary layer separation along the face of the cylinder which in turn results in the formation of vortex 1. Due to the action of vortex 1, the local pressures near the bed around the cylinder become higher than the upstream pressure at the same level above the bed.

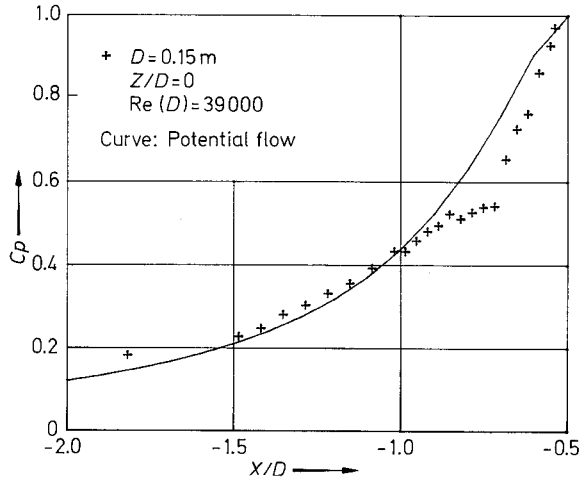

Fig. 4. Pressure coefficient along the line of symmetry upstream of a cylinder

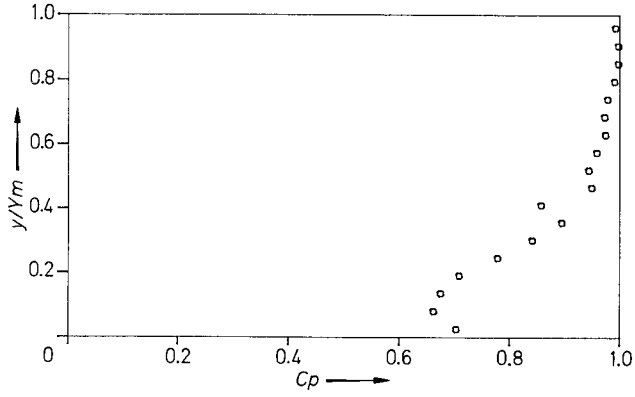

Fig. 5. Pressure distribution along the stagnation line at the upstream face of a cylinder at $Re(D) = 39{,}000$ ($D = 0.15$ m)

Table 1. Basic flow conditions

U (m/s)	Um (m/s)	Ym (m)	δ (m)	u_* (m/s)	v/u_* (mm)	v/u_*^2 (s)	$Re(D)$ $\times 10^{-3}$	$Re(l)$ $\times 10^{-6}$
0.3	0.26	0.2	0.2	0.012	0.1	0.01	39	46

3.4.2 Velocity distributions

The streamwise mean velocity distributions were measured along the plane of symmetry upstream of the cylinder. The measurements were taken at 14 different stations in the region $-2.5 < X/D < -0.63$. The distributions agreed well with the logarithmic and wake universal laws in the region

$-2.5 < X/D < -1.2$, whereas in the region $-1.1 < X/D < -0.87$ the distributions were significantly influenced by the adverse pressure gradient set up by the cylinder. However, if the boundary layer thickness, δ is replaced by a parameter Δ defined as

$$\Delta = \int_0^{\delta} (U-u)/u_* \, dy$$

a more or less "universal distribution" is obtained (Fig. 6).

The main boundary layer parameters i.e. displacement and momentum thicknesses were calculated from the velocity distributions. At the position of the primary separation point the shape factor reached a maximum value of 1.83. For the case of a 2-D boundary layer flow, separation point is normally signified with larger values of shape factor. The disagreement is mainly due to 3-D character of the flow which influences the velocity distributions. The boundary layer parameters were used to estimate the order of magnitude of the various terms in the three-dimensional momentum integral equation along the plane of symmetry, given by Johnston (1957) i.e. Eq. (1.2).

$$\underset{\text{I}}{\frac{\partial \Theta_x}{\partial x}} + \underset{\text{IV}}{\frac{\partial \theta_{xz}}{\partial z}} + \underset{\text{III}}{(2\theta_x + \delta_d)\frac{1}{U}\frac{\partial U}{\partial x}} + \underset{\text{V}}{\frac{\theta_x}{U}\frac{\partial W}{\partial x}} = \underset{\text{II}}{\frac{\tau_{ox}}{\varrho U^2}}. \qquad (1.2)$$

In which, $\theta_{xz} = (1/U^2) \int_0^{\infty} (U-u)\, w \, dy$ and τ_{ox} = bed shear stress.

The values of shear velocity were obtained from Clauser plot (Clauser 1954). The results showed that the skewness (IV) and divergence (V) terms in Eq. (1.2) are of the same order of magnitude as the other terms in the equation and their magnitude increase as the primary separation point is approached. In the vicinity of separation, the skewness term is somewhat larger than the divergence term. Consequently, neither of the terms can be ignored for the case of a 3-D boundary layer flow under adverse pressure gradient.

The instantaneous velocity distributions obtained by hydrogen bubble method at various positions upstream of the cylinder, confirm the existence of a complex inrush-ejection process in the separated flow region. The ejected fluid from the bed boundary travels almost the entire boundary layer thickness. The process is significantly affected by shedding of the horse-shoe vortices. An example of the distributions for various times at station $X/D = -1.06$ is shown in Fig. 7. For the purpose of comparison the mean velocity distribution measured by means of a hot-film probe is also plotted in the figure. The distributions have inflexion points similar to those observed during so-called 'bursting' in turbulent flow. The low and high velocity regions correspond to ejection and inrush phase, respectively. During each cycle of the horse-shoe vortex formation, vorticity becomes concentrated along the bed at positive bifurcation points (i.e. "attachment") whereas at negative bifuration points (i.e. "separation"), the vorticity is transported to regions away from the bed. The transport and concentration of vorticity results to a complex disturbing mechanism which is similar to the well known bursting process.

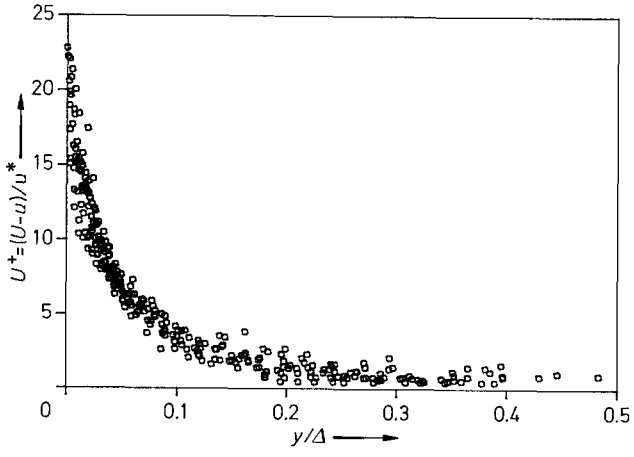

Fig. 6. Streamwise velocity distributions upstream of a cylinder at stations $X/D = -2.5$ to -0.83

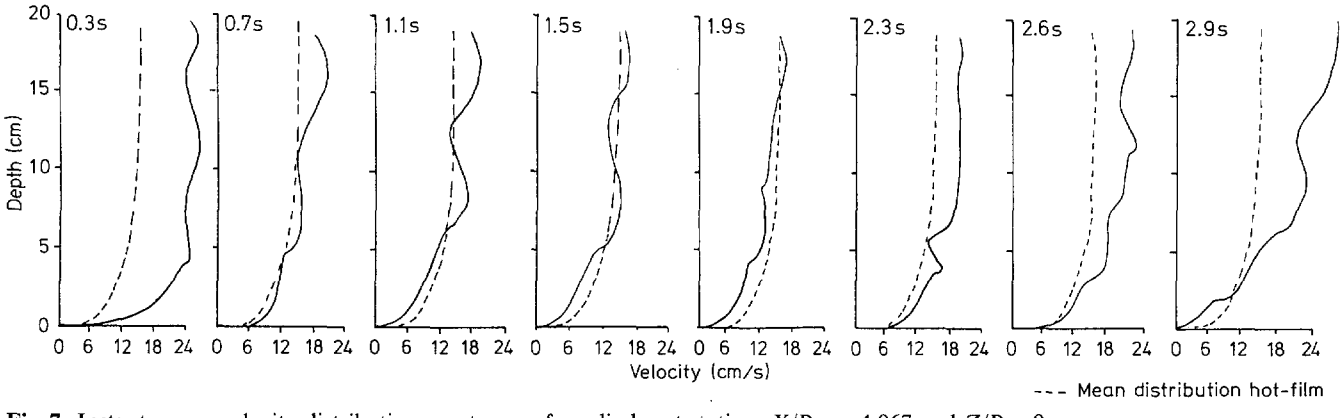

Fig. 7. Instantaneous velocity distributions upstream of a cylinder at station: $X/D = -1.067$ and $Z/D = 0$

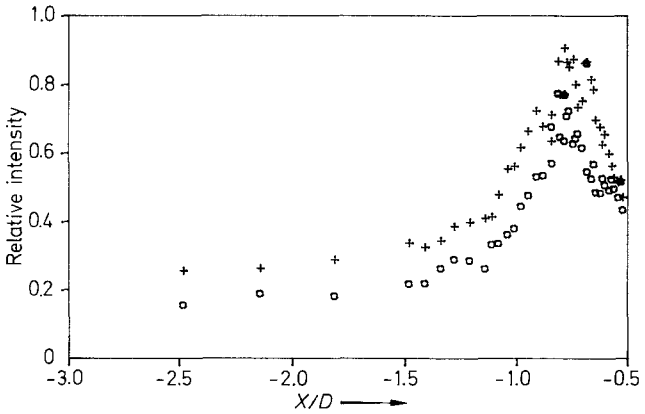

Fig. 8. Turbulence intensity along the plane of symmetry upstream of a cylinder at $Re(D) = 39{,}000$, $D = 0.15$; + $y/Ym = 0.005$, o $y/Ym = 0.025$

Table 2. Skewness and flatness factors

Source	Channel flow		Present study	
$Y+$	*Su*	*Fu*	*Su*	*Fu*
10	+0.2	2.2	+0.15	2.5
50	−0.5	3	−0.15	2.5

3.4.3 Statistical analysis of instantaneous velocity signals

The measurements were taken at 45 different stations along the line of symmetry upstream of the cylinder, in the region $-2.5 < X/D < -0.54$. At each station the velocities were measured at two different points above the bed i.e. $y/Ym = 0.005$ and $y/Ym = 0.025$ ($Ym = \delta = 20$ cm). Upstream of the primary separation point, the two points are roughly located in the buffer and logarithmic regions. Each velocity record was 100 s long, sampled with a frequency of 100 Hz. The flow visualization results indicated that the mean flow direction in the separated flow region close to the bed, is mainly in the reversed direction. In this region the velocity signals were characterized by two distinct low and high regions. Low velocities appeared as regions of low plateaus in the record. The character of the velocity signals in these regions were found to be distinctively different from the rest of the signal. Generally, in the separated upstream region, during 70–90% of the record time, the flow was reversed. The flow directions found by the foregoing method were consistent with flow visualization results.

The distribution of relative turbulence intensity is shown in Fig. 8. As the cylinder is approached, the intensity increases until a maximum value is reached in the vicinity of the primary separation point. In the region $-2.5 < X/D < -1.4$, the distribution exhibits values comparable to those reported in the literature for turbulent boundary layers along a smooth wall. The intensities in the region $-0.7 < X/D < -0.5$ are one order magnitude larger than in the region $-0.83 < X/D < -0.7$. The regions correspond to the locations of primary vortices 2 and 4, respectively.

The distribution of flatness (*Su*) and skewness factors were found to have the same trend as that given in Fig. 8. In the region $-3 < X/D < -1$, both factors were almost independent of the normalized distance X/D. In Table 2, a comparison is made between the *Su* and *Fu* values of the present study and those measured in a channel flow (Johansson and Alfredsson 1986). The comparison indicates that the turbulent structure of the flow in the region $-3 < X/D < -1$ is similar to the structure of turbulent wall bounded shear flows. In the separated region, the distribution of *Fu* and *Su* factors were quite high (found 2.5–14 and 0.5–4, respectively). The maximum values occurred near the primary separation point. The high values of *Fu* reveal the intermittent character of the flow. In the separated region i.e. $-0.83 < X/D < -0.5$, the high values of the factors are characteristic of the complex vortex motion in this region where the flow structure is significantly different from that of the non-separated region.

The flow visualization results indicated that the horse-shoe vortices upstream of the cylinder are not significantly influenced by the wake flow downstream of the cylinder. This was also verified by measurement of the instantaneous velocities upstream of an elongated cylinder, along the line of symmetry, for which case the downstream vortex shedding was eliminated.

The auto-correlation plot of the velocity signals in the separated flow region (i.e. $-0.83 < X/D < -0.54$) revealed the periodical nature of the flow. The results of spectrum analysis lead to the following conclusions:

(1) The energy is concentrated in the low frequency range 0–5 Hz.
(2) Different vortices are shed with the same frequency. Vortices 3 and 5 are shed at higher frequencies than those of vortices 1, 2 and 4.
(3) The influence of the horse-shoe vortices extends well upstream of the primary separation point to region $-1.8 < X/D < -0.54$.
(4) The frequency range found for the case of the elongated cylinder was remarkably similar to those found for the circular cylinder.

The computed auto-correlation functions were used to calculate the Eulerian integral scale defined by

$$T_E = \int_0^\infty R_{uu}\, dt. \tag{1.3}$$

The method is suitable only if the correlation function shows no definite periodicity. Thus, prior to the calculations periodical components were removed from the raw data. The length scale was obtained through the multiplication of T_E by the local mean velocity (Taylor hypothesis). In the region $-2.5 < X/D < -0.9$, this length scale is more or less constant and comparable with the boundary layer thickness

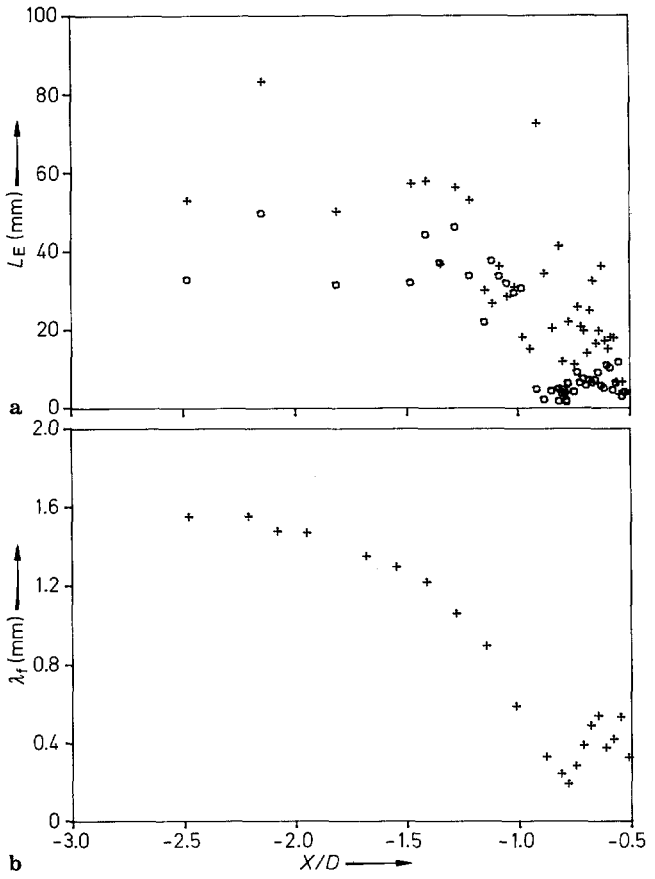

Fig. 9. **a** Eulerian integral length scale along the plane of symmetry upstream of a cylinder at $Re(D) = 39{,}000$, $D = 0.15$ m; + $y/Ym = 0.005$, o $y/Ym = 0.025$; **b** Eulerian micro length scale along the plane of symmetry upstream of a cylinder at $Re(D) = 39{,}000$, $D = 0.15$ m; + $y/Ym = 0.005$

$\delta = 0.2$ m or the diameter of the cylinder $D = 0.15$ m (Fig. 9 a). As the point of separation is approached, the scales become finer. In the separated flow region the existence of a varying length scale is revealed which is characteristic of the horse-shoe vortices. The range of scales are in good agreement with the size of vortices estimated from the flow visualization.

An estimate of the small scale eddies (Taylor micro scale) was obtained from a direct method given by Townsend (Hinze 1975) given as

$$\frac{2}{\lambda_f^2} = \frac{1}{\overline{U}^2}\frac{1}{\overline{u^2}}\overline{\left(\frac{\partial u}{\partial t}\right)^2}. \tag{1.4}$$

The values of λ_f were estimated from instantaneous velocity signals sampled with a frequency of 210 Hz. Taylor's hypothesis is invoked in the above definition. The distribution of the micro length scale is shown in Fig. 9 b. As the cylinder is approached the scale decreases until a minimum value is reached in the vicinity of the primary separation point. In the separated region the distribution exhibits two minima and maxima which is assumed to be due to the action of horse-shoe vortices.

Table 3. The duration of flow reversal

X/D	% < 0.65 times local mean velocity		
	y/Ym		
	0.025	0.1	0.9
0.57	34	30	31
1.3	38	35	30
2	37	25	29
8	5.5	6	6

The estimated values of both the Eulerian integral scale and the micro scale are only typical scales and they give an indication of the order of magnitude. Taylor hypothesis is not also entirely valid for this case. The scales found in the separated region of flow should be accepted with some reservation.

3.5 Flow measurements: downstream region

The main difficulty encountered in one point velocity measurements in the wake of the cylinder is the detection of local flow direction. The same method applied to the upstream separation region was adopted. With the hot-film aligned in the main flow direction, velocity records of 200 s duration were obtained at each point. The velocity signals were then analysed in order to determine the duration of flow reversal which is characterized by low frequency fluctuations appearing as a low plateau. The mean local velocity was used as a base of comparison. At each point, velocities K times the mean velocity were classified as those corresponding to flow reversal. The final result depends to some degree on the choice of the constant K. Analysis of the velocity signals at various locations in the flow, showed that $K = 0.65$ is a reasonable choice. Data were sampled accordingly. The result of this analysis at four different stations ($Z/D = 0$) are shown in Table 3. The values given in the table represent the percentage of time for which the comparison criterion was satisfied. In the region $X/D < 2$, the duration of flow reversal is about 30% of the total record time. At station $X/D = 8$, negligible flow change occurs.

The measurements were confined to the region close to the cylinder in the range $-0.5 < X/D < 8$. The velocity profiles in various different horizontal and vertical planes were measured by means of hot-film anemometry. In order to gain more insight into the change of flow pattern the velocity distributions were measured in both flow and reversed flow directions. Although the results obtained could not be interpreted in terms of different flow patterns, they indicated the existence of an equally strong flow in the reversed flow direction. An example is given in Fig. 10 for the measuring station located at $X/D = 0.57$ and $Z/D = 0$. The distribution of maximum velocities is also shown. The velocities are normalized with the maximum velocity of the mean distribution. The velocities are remarkably similar in both directions. The

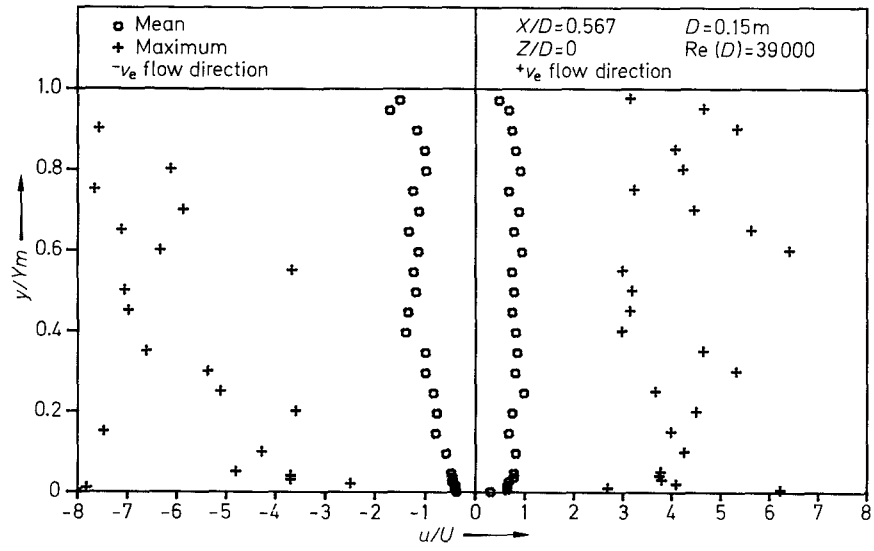

Fig. 10. Velocity distributions downstream of a cylinder in flow and reversed flow direction

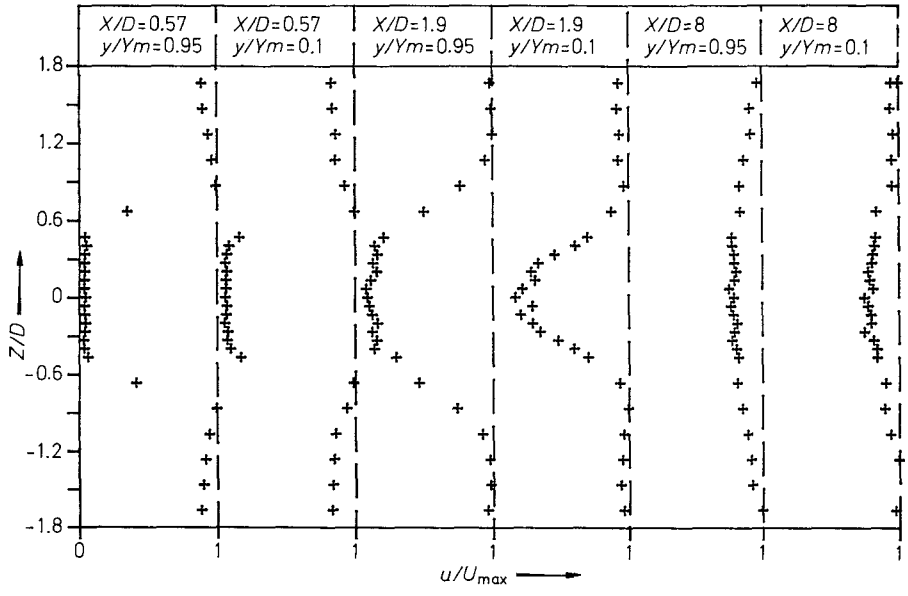

Fig. 11. Streamwise velocity distributions downstream of a cylinder

maximum flow velocities were found to be generally several orders of magnitude larger than the mean velocities, implying a high level of turbulence intensity in the wake of the cylinder.

In order to assess the influence of the bed boundary layer on the development of the wake flow, velocity distributions were measured at different horizontal planes, one located at $y/Ym = 0.95$ and the other $y/Ym = 0.1$, above the flume bed. The results of measurements are shown in Fig. 11. The data are normalized with the maximum velocity. In the region $X/D \leq 1.9$, the mean distributions are considerably different from those at $y/Ym = 0.95$. The width of the wake is smaller near the flume bed. The width of the wake, the momentum thickness and the drag coefficients were also computed from the velocity distribution. For the case of 2-dimensional wake at $Re(D) = 39{,}000$, the drag coefficient and momentum thickness are about 1.2 and 9 cm, respectivley. The experimentally found θ and C_d values already at $X/D = 8$ ($Cd = 1.15$, $\theta = 8.5$ cm) are close to the expected values, although the mean flow statistics at this position are far from complying with the similarity conditions.

The decay of maximum velocity deficiency downstream of the cylinder is shown in Fig. 12. For comparison, data found by Melville (1975) are included. The decay at distance $X/D \leq 8$, i.e. in the near wake, seems to be well approximated by a linear equation in contrast to the inverse square root dependence in the far wake. The width of the wake was found to increase almost linearly with the distance for both $y/Ym = 0.1$ and $y/Ym = 0.95$. According to the similarity solution, the width increases with square root of the dis-

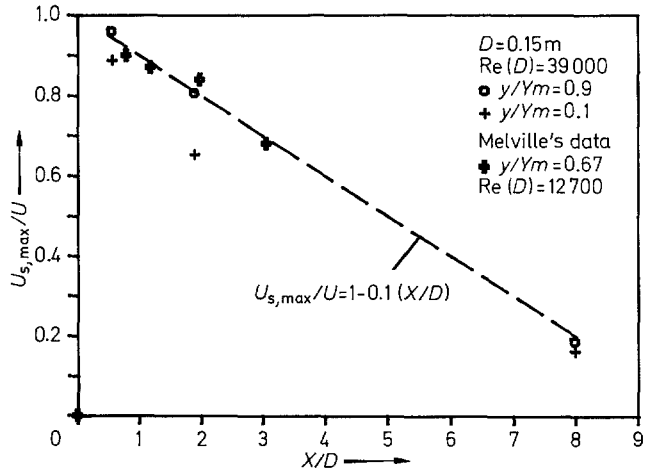

Fig. 12. Longitudinal decay of maximum velocity deficiency downstream of a cylinder

tance. Hence, both the decay of maximum velocity deficiency and spread of wake is much faster in the region $X/D \leq 8$, as compared to the similarity region of the wake.

The dominant shedding frequency of the primary vortices was found to be about 0.33 Hz. This value compares well with 0.32 Hz, the Strouhal frequency at $Re(D) = 39{,}000$. The shedding frequency in the range of $0.1 < y/Ym < 0.9$ is constant.

The results of statistical analysis of the velocity signals collected at various locations indicated that:

(1) In the region $0.5 < X/D < 0.9$, *Su* and *Fu* factors are high and differ significantly from the values of a Gaussian distribution. The flow in this region has a strong intermittent nature. Near the flume bed where the wake flow is influenced by the bed boundary the intermittency is lower than the other regions.
(2) At normalized distances $X/D > 5.5$, both *Su* and *Fu* factors become practically independent from the downstream distance.

3.6 Bed shear stresses

The bed shear stresses were measured at different stations located along the line of 0°, 45°, 90° and 110° measured from the forward stagnation point. At each station the Preston tube was aligned along the main flow direction. The results of measurements along the line of symmetry upstream of the cylinder, were also compared with the estimates obtained from Clauser plot, Ludwieg and Tillmann (1950) equation given by

$$C_f = \frac{0.246 * 10^{-0.678\,\mathrm{H}}}{Re(\theta)^{0.268}} \tag{1.5}$$

and by measuring the velocity gradient near the bed (at $y/Ym = 0.0025$). The first two methods were used only in the non-separated region of the flow.

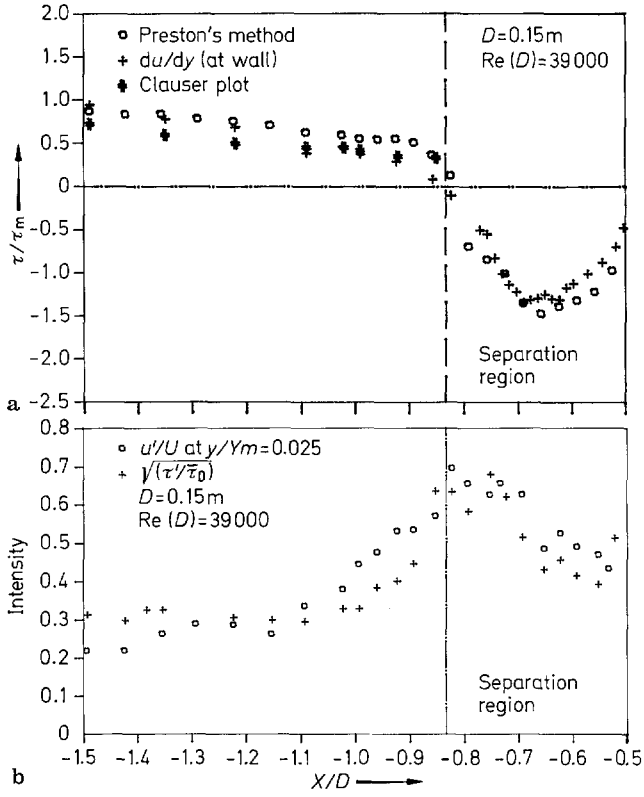

Fig. 13. a Mean bed shear stresses along the line of symmetry upstream of a cylinder; **b** turbulence intensity of bed shear stresses and velocity along the line of symmetry upstream of a cylinder

In Fig. 13a comparison is made between the different methods used. The data are normalized with the mean shear stress (τ_m) at station $X/D = -2.5$. The shear stresses are reduced as the cylinder is approached. The minimum value is reached at the point $X/D = -0.83$ which was identified before, as the primary separation point. The values obtained from Eq. (1.5) are not plotted in the figure, as they were identical with those obtained by the Preston method. The good agreement between the different methods confirm the validity of the Preston method and the universal constants given by Patel (1965), for the case of 3-dimensional boundary layer with adverse gradient. Despite the lack of dynamic similarity, Preston method appears to give consistent values of bed shear stresses in the separated upstream region. The shear stress distribution in this region exhibited a maximum value at the mean locations of horse-shoe vortices 3 and 4. The maximum value was found to be 1.5 times τ_m. Significant increase of shear stresses occur close to the cylinder along the lines of 45° and 90°. The maximum shear stresses at these locations were about 4.5 and 3.5 times the undisturbed shear stress, respectively. Under the horse-shoe vortices the maximum shear stress reaches a value of about 2.5 times τ_m.

The relative bed shear stress fluctuations intensity $\tau'/\overline{\tau_0}$ and the corresponding near-wall turbulence intensity are shown in Fig. 13b.

4 Conclusions

The flow field around a circular cylinder has been investigated experimentally in a fully developed turbulent open channel flow. Hydrogen bubble flow visualization and hot-film measurements were carried out. The main flow feature upstream of the cylinder is a three-dimensional boundary layer separation. The flow field in the separated region is characterized by a system of horse-shoe vortices which are shed quasi-periodically. This vortex system is practically independent of the wake vortices. The number of vortices increases with increasing Reynolds number and the complexity of the flow grows. The dimensions of the vortex system were found to be independent of Reynolds number and are primarily determined by the diameter of the cylinder. The topology of the separated flow contains several separation and attachment lines, and the location of these change with Reynolds number. At the primary boundary layer separation point the value of shape factor is lower than its two-dimensional counterpart. The mean velocity distributions along the plane of symmetry agree well with the logarithmic and wake universal laws in the region $-2.5 < X/D < -1.2$, whereas in region $-1.1 < X/D < -0.87$, the distributions are significantly influenced by the adverse pressure gradient set up by the cylinder. However, the wake law gives a more or less "universal" distribution for both regions if the boundary layer thickness is replaced by $\int (U-u)/u_* \, dy$.

The turbulent structure of the flow in the region $-3 < X/D < -1$ was found to be similar to the structure of turbulent wall bounded shear flow. In separated flow region the statistical moments reach very high values which are characteristic for the complex vortex formation in this region. Horse-shoe vortices 4 and 5 were found to cause greater degree of intermittency than the other vortices. The relative turbulence intensity increases considerably under the vortices and it reaches a maximum value of about 85%.

The Eulerian integral and micro length scales are both reduced in the separated upstream region. The size of horse-shoe vortices is of the same order of magnitude as the integral scale.

The primary wake vortices are shed with constant frequency in the wake of the cylinder where the flow patterns in a vertical plane change with the phase of vortex shedding process (for a constant Reynolds number). Both the decay of maximum velocity deficiency and spread of wake is much faster in the region $X/D \leq 8$, as compared to the similarity region of the wake. The former was found to decrease approximately linearly within this region. Near the flume bed, the flow separation from the sides of the cylinder is displaced forward to a point located at 90°. The width of the wake also decreases as the bed boundary is approached.

The flow in the region $0.5 < X/D < 3$ has a strong intermittent nature and the values of the higher statistical moments are high. At $X/D > 5$ the moments become independent of the downstream distance and the wake becomes more or less fully turbulent.

Acknowledgement

This paper is a part of a research program in river erosion. The project was sponsored by the Swedish Council for Building Research. This support is gratefully acknowledged. The author also wishes to thank Prof. A. Johansson and Prof. Klas Cederwall for their guidance and encouragement.

References

Belik, L. 1973: The secondary flow about circular cylinder mounted normal to a flat wall. Aeronaut. Q. 24, 47–54

Clauser, F. H. 1954: Turbulent boundary layers in adverse pressure gradient. J. Aeronaut. Sci. 21, 91–108

Dallmann, U. 1983: Topological structure of three-dimensional vortex flow separation. AIAA 16th fluid plasma dyn. conf. Danvers/MA: American Institute of Aeronautics and Astronautics

Dargahi, B. 1983: Local scouring around bridge piers – A review of practice and theory. Hydraulics lab. Bull. No. 114, Stockholm: R. Inst. Tech.

Goldstein, R. J.; Karni, J. 1984: The effect of a wall boundary layer on local mass transfer from a cylinder in crossflow. J. Heat Transfer 106, 260–267

Hinze, J. O. 1975: Turbulence. New York: McGraw-Hill

Hunt, J. C. R.; Abell, C. J.; Peterka, S. A.; Woo, H. 1978: Studies of the flow around free or surface-mounted obstacles; applying topology to flow visualization. J. Fluid Mech. 86, 179–200

Johannson, A. V.; Alfredsson, P. H. 1986: Structure of turbulent channel flows. In: Encyclopedia of fluid mechanics (ed. Cheremisinoff, N. P.) pp. 825–869. Houston, London, Paris, Tokyo: Gulf

Johnston, P. J. 1957: Three-dimensional turbulent boundary layer. Gas Turbine Lab. Report No. 39

Lighthill, M. J. 1963: Introduction. Boundary layer theory. In: Laminar boundary layer (ed. Rosenhead, L. R.) pp. 48–88. Oxford University Press

Ludwieg, H.; Tillmann, W. 1950: Investigations of the wall shearing stress in turbulent boundary layers. NACA TM 1285

Maskell, E. G. 1955: Flow separation in three-dimensions. Royal Aircraft Establishment, Faranborough, Report No. Aero 2565

Melville, B. W. 1975: Local scour at bridge sites. University of Auckland, Report No. 117

Patel, V. C. 1965: Calibration of the Preston tube and limitations on its use in pressure gradients. J. Fluid Mech. 23, 185–208

Perry, A. E. Fairlie, B. D. 1974: Critical points in flow patterns. Advances in geophysics. 18B. New York: Academic Press

Perry A. E., Steiner, T. R. 1987: Large-scale vortex structures in turbulent wakes behind bluff bodies. Part 1. Vortex formation processes. J. Fluid Mech. 174, 233–270

Preston, J. H. 1954: The determination of turbulent skin friction by means of pitot tubes. J. Roy. Aeronaut. Soc. 58, 109–121

Roper, A. T. 1967: A cylinder in a shear flow. Colorado State University

Roshko, A. 1953: On the development of turbulent wakes from vortex streets. NACA TN 2913

Schraub, F. A.; Kline, S. J.; Henry, J.; Runstadler, P. W.; Littel, A. 1965: Use of hydrogen bubbles for quantitative determination of time-dependent velocity fields in low-speed water flows. J. Basic Eng. 87, 429–444

Schwind, R. G. 1962: The three dimensional boundary layer near a strut. Gas Turbine Laboratory, Report No. 67

Smith, D. W.; Walker, J. E. 1958: Skin-friction measurements in incompressible flow. NACA TN 4231

Tobak, M.; Peake, D. J. 1982: Topology of three-dimensional separated flow. Annu. Rev. Fluid Mech. 14, 51–85

Wei, T.; Smith, C. R. 1986: Secondary vortices in the wake of circular cylinders. J. Fluid Mech. 169, 513–533

Received February 27, 1989